Supporting Information

Machine Learning-Assisted Ag-TiO_2 SERS Platform for Intraoperative Osteomyelitis Diagnosis

Yunfan Chen[a,1], Tengjiao Zhu[b,c,1], Langran Wang[b,c], Yechen Wang[a], Qizhao Tan[b,c], Yun Tian[b,c], Lu Zhao[a,*], Qi An[a,*], Gao Si[b,c,*]

[a]School of Materials Science and Technology, China University of Geosciences, Beijing 100083, China

[b]Department of Orthopedics, Peking University Third Hospital, Beijing 100191, China

[c]Engineering Research Center of Bone and Joint Precision Medicine, Beijing, China

*Corresponding author.

E-mail address: si_gao@126.com (S.Gao); lzhao@cugb.edu.cn (L.Zhao); an@cugb.edu.cn (Q.An)

[1]These authors contributed to the work equally and should be regarded as co-first authors.

Method S1. Calculation of EF values on Ag, and Ag-TiO_2.

The EF of Ag and Ag-TiO_2 substrates was calculated according to Equation (1)[1]:

$$EF = \frac{I_{SERS}/N_{SERS}}{I_{bulk}/N_{bulk}} = \frac{I_{SERS}}{I_{bulk}} \times \frac{\rho h A_{sub}}{cVM} \quad (1)$$

In the experiments, 5 μL of WSIF solution was drop-cast onto a Si wafer with an effective sampling area of A_{Sub} = 0.02 cm^2. and the laser confocal depth was set to h = 2 μm. The molecular parameters of representative WSIF components were used for EF estimation: tyrosine (M= 181.19 g/mol, ρ = 1.46 $g \cdot cm^{-3}$), uric acid (M= 168.11 g/mol, ρ = 1.89 $g \cdot cm^{-3}$), phenylalanine (M= 165.19 g/mol, ρ = 1.29 $g \cdot cm^{-3}$). The Raman peaks at 854 cm^{-1} (tyrosine), 893 cm^{-1} (uric acid), and 1020 cm^{-1} (phenylalanine) were selected to evaluate the corresponding EFs.

$EF_{Ag(tyrosine)} = 4.63 \times 10^5$

$EF_{Ag\text{-}TiO2(tyrosine)} = 1.61 \times 10^6$

$EF_{Ag(uric\ acid)} = 4.77 \times 10^5$

$EF_{Ag\text{-}TiO2(uric\ acid)} = 1.79 \times 10^6$

$EF_{Ag\text{-}TiO2(phenylalanine)} = 5.70 \times 10^5$

$EF_{Ag\text{-}TiO2(phenylalanine)} = 6.17 \times 10^6$

Method S2. Calculation of the chemically enhanced specific gravity (ρ_{CT}) of probe molecules.

The contribution of CM to SERS enhancement can be quantitatively characterized by the chemical-enhancement specific gravity, ρ_{CT}, larger values indicate a greater relative contribution of CT to the observed SERS intensity[2, 3]. For a given vibrational band κ, $\rho_{CT}(\kappa)$ is defined as:

$$\rho_{CT}(\kappa) = \frac{I^{\kappa}(CT) - I^{\kappa}(SPR)}{I^{\kappa}(CT) + I^{0}(SPR)} \quad (2)$$

where $I^{\kappa}(CT)$ is the observed intensity of a non-totally symmetric vibrational band κ, for which CT is expected to contribute significantly to the SERS intensity; $I^{\kappa}(SPR)$ is the contribution of the EM mechanism to the same band κ; $I^{0}(SPR)$ is the intensity of a totally symmetric reference band that is assumed to arise predominantly from the EM mechanism. If the κ-band is totally symmetric, the contribution from SPR dominate the intensity, and $I^{\kappa}(SPR) = I^{0}(SPR)$. If a band κ is purely totally symmetric, its intensity is dominated by SPR and $I^{\kappa}(CT) \approx 0$. Conversely, for strongly CT-enhanced (non-totally symmetric) bands $I^{\kappa}(SPR)$ is often small and can be neglected in first approximation. $\rho_{CT}(\kappa) = 0$ indicates negligible CT contribution; $\rho_{CT}(\kappa) = 1$ indicates CT strongly dominates the observed intensity. Intermediate values reflect mixed contributions. For quantification of the CM contribution we computed $\rho_{CT}(\kappa)$ according to Eq. (2). Peak areas were integrated for the CT-sensitive bands and totally-symmetric reference bands using the following windows (cm^{-1}): tyrosine I^{κ} 846, I^{0} 1609; uric acid I^{κ} 907, I^{0} 1022; phenylalanine I^{κ} 1045, I^{0} 1003.

Method S3. Calculation of the work functions of TiO_2 and Ag-TiO_2.

The work functions (Φ) of TiO_2 and Ag-TiO_2 were determined from the ultraviolet photoelectron spectroscopy (UPS) spectra. According to the standard equation[4]:

$$\Phi = 21.22\ eV - (E_{Fermi} - E_{cutoff}) \quad (3)$$

where E_{Fermi} is the Fermi edge and E_{cutoff} is the secondary electron cutoff. Using this method, the work functions of TiO_2 and Ag-TiO_2 were calculated to be -4.75 eV and -3.73 eV, respectively.

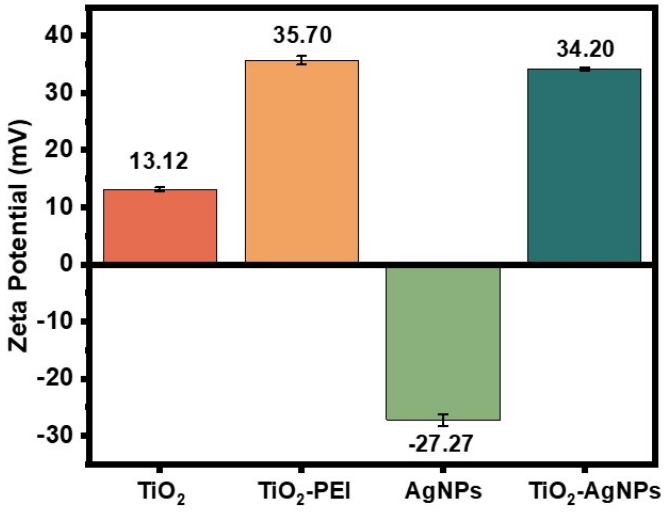

Figure S1. Zeta potenial of TiO_2, TiO_2-PEI, AgNPs and Ag-TiO_2.

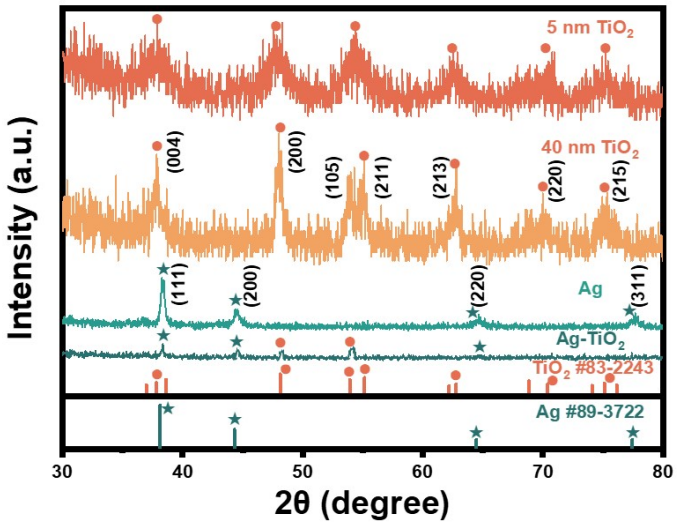

Figure S2. XRD of TiO_2, AgNPs and Ag-TiO_2.

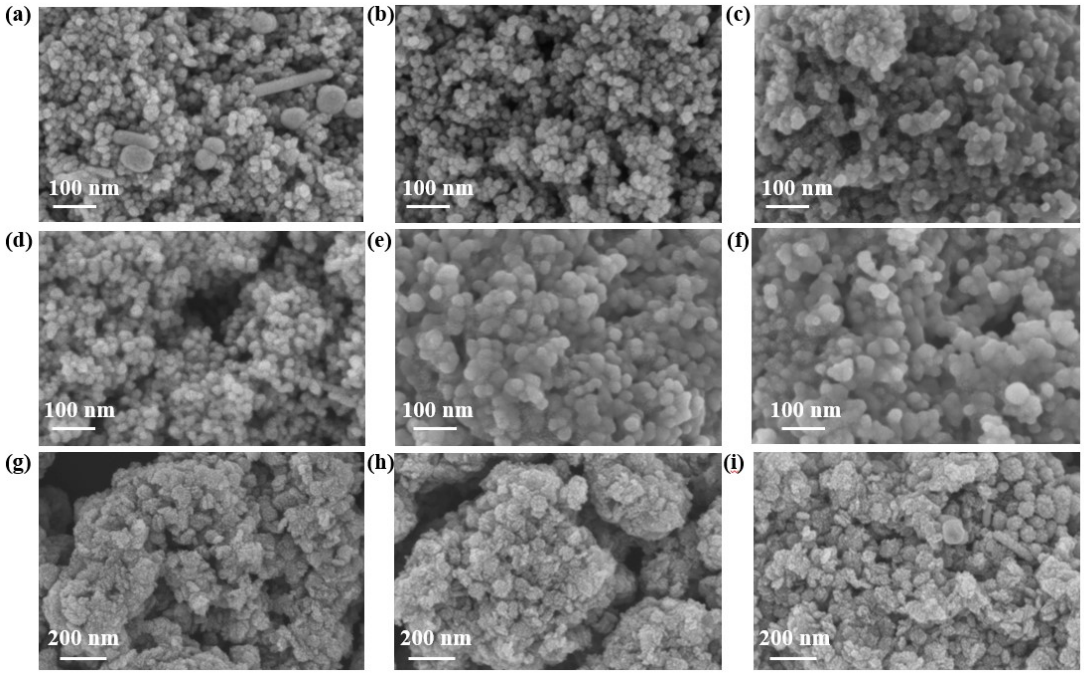

Figure S3. SEM images of Ag-TiO_2 composite substrates under different preparation conditions: (a-c) 0.01 g TiO_2 (20 nm) assembled with one, two, and three layers of AgNPs; (d-f) 20 nm TiO_2 with different masses (5 mg, 10 mg, and 15 mg) combined with one layer of AgNPs; (g-i) 0.01 g TiO_2 (5 nm) assembled with one, two, and three layers of AgNPs.

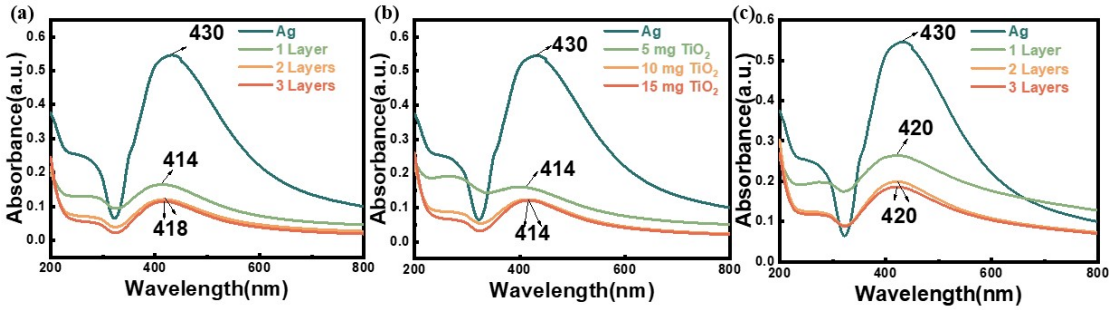

Figure S4. UV–vis absorption spectra of Ag-TiO_2 composite substrates under different preparation conditions: (a) 0.01 g TiO_2 (20 nm) assembled with one, two, and three layers of AgNPs; (b) 20 nm TiO_2 with different masses (5 mg, 10 mg, and 15 mg) combined with one layer of AgNPs; (c) 0.01 g TiO_2 (5 nm) assembled with one, two, and three layers of AgNPs.

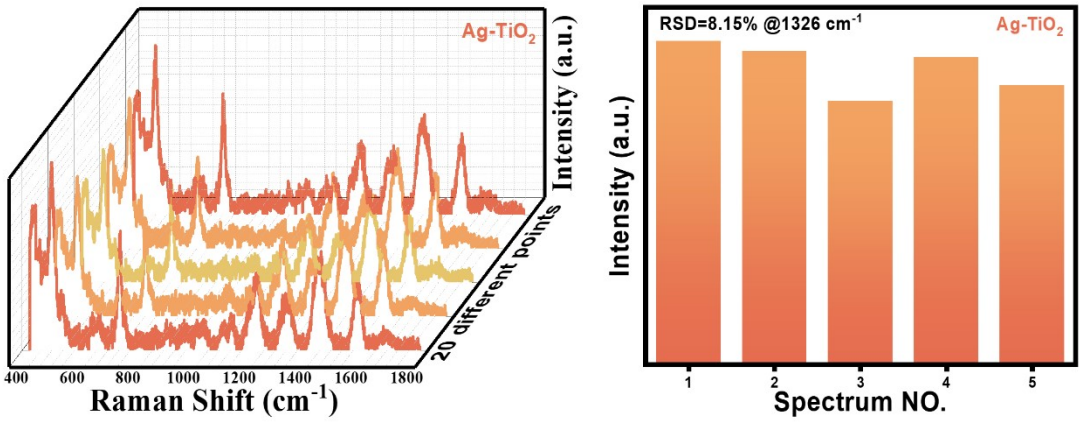

Figure S5. (a) Batch-to-batch WSIF SERS spectra obtained from five independently prepared Ag-TiO_2 substrates. (b) Corresponding RSD of the 1326 cm^{-1} Raman band, indicating good batch-to-batch reproducibility.

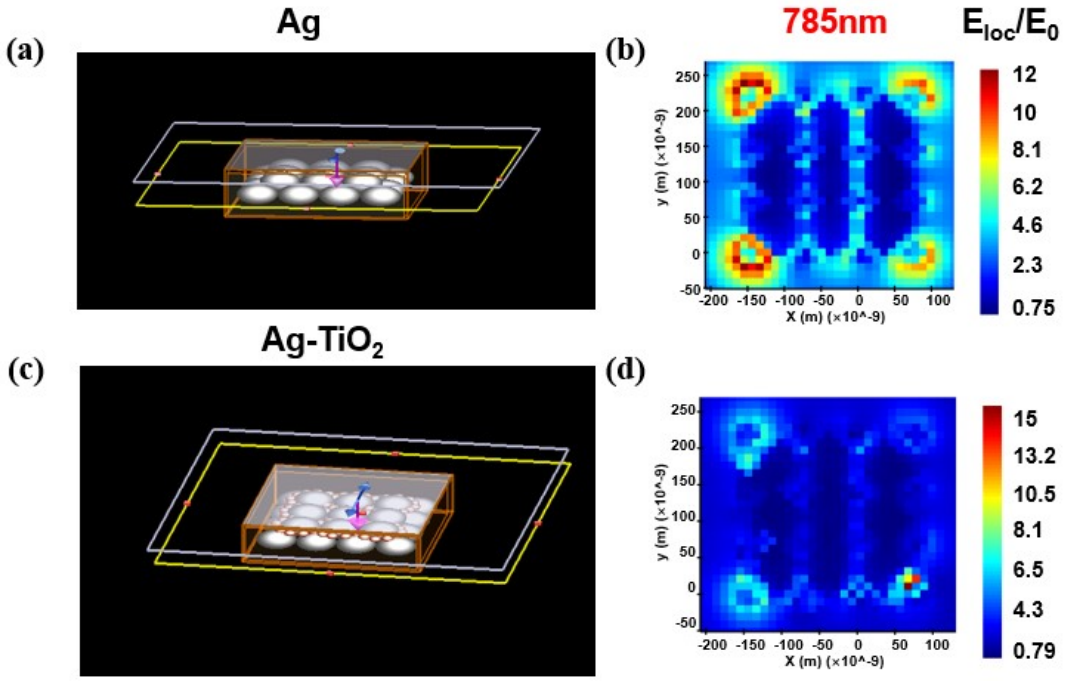

Figure S6. (a) FDTD model of Ag substrate. (b) Simulated electric field distribution of Ag substrate. (c) FDTD model of Ag-TiO_2 composite substrate. (d) Simulated electric field distribution of Ag-TiO_2 composite substrate.

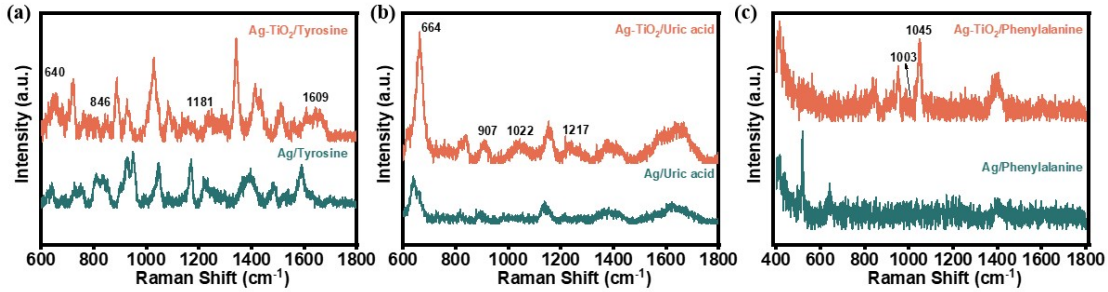

Figure S7. (a) SERS spectra of tyrosine acquired on Ag and Ag-TiO_2 substrates. (b) SERS spectra of uric acid acquired on Ag and Ag-TiO_2 substrates. (c) SERS spectra of phenylalanine acquired on Ag and Ag-TiO_2 substrates.

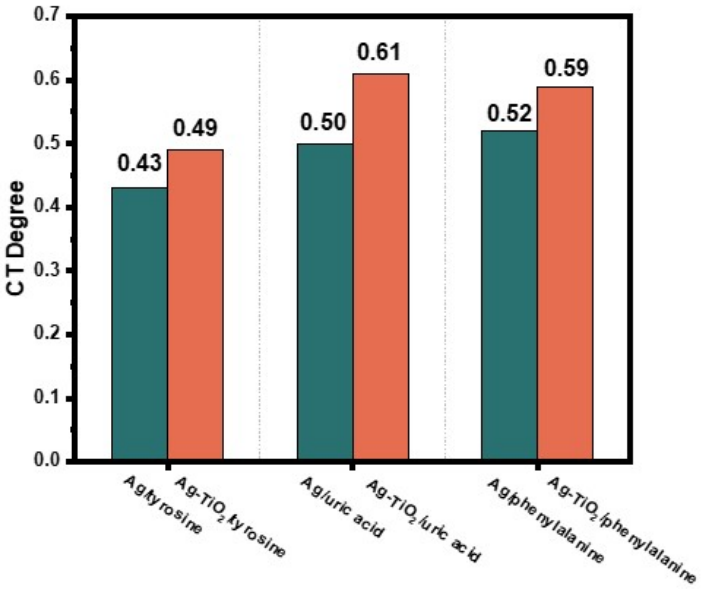

Figure S8. CT degree (ρ_{CT}) of the tyrosine, uric acid and phenylalanine in Ag and Ag-TiO_2.

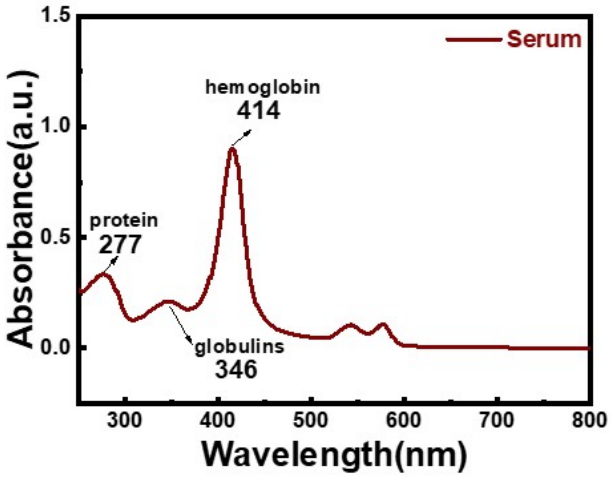

Figure S9. UV-vis absorption spectra of WSIF.

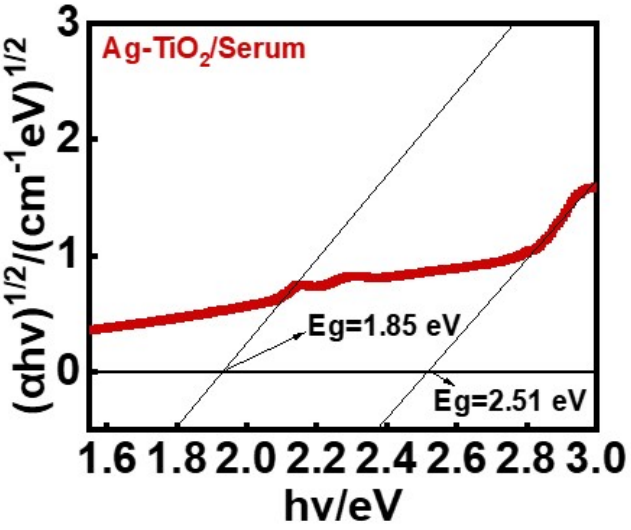

Figure S10. Tauc plots of $(\alpha h\nu)^{1/2}$ versus photon energy (hν) for Ag-TiO_2/ WSIF hybrid system, used to estimate the optical bandgap.

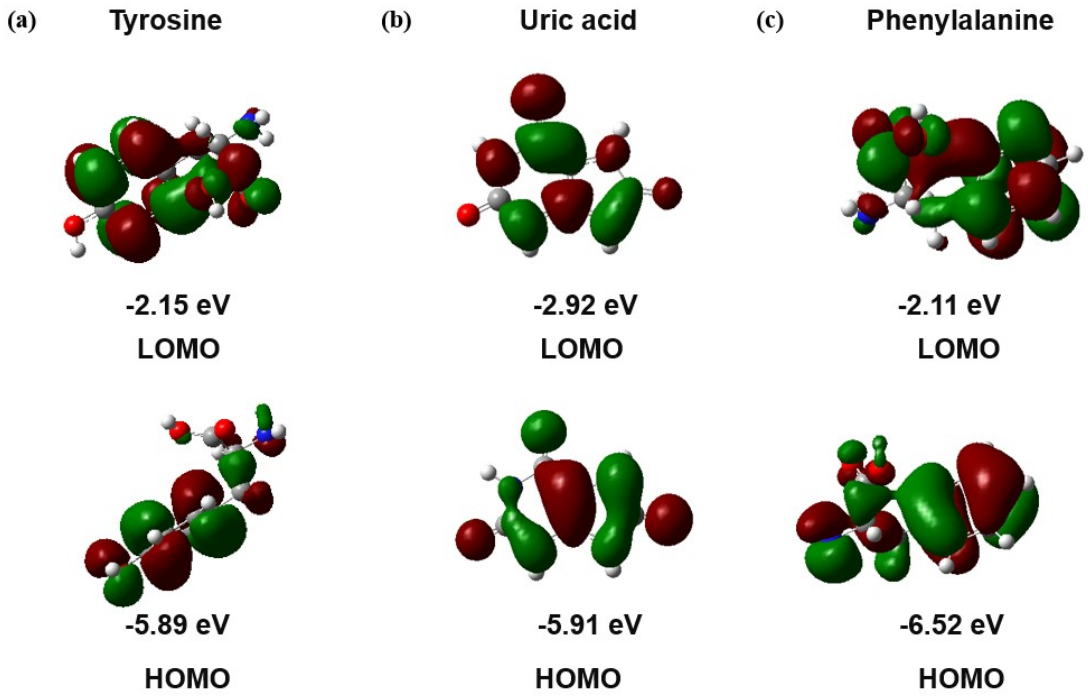

Figure S11. Gaussian-simulated HOMO and LUMO energy levels of (a) tyrosine, (b) uric acid, and (c) phenylalanine, showing their relative frontier orbital positions relevant to charge-transfer pathways.

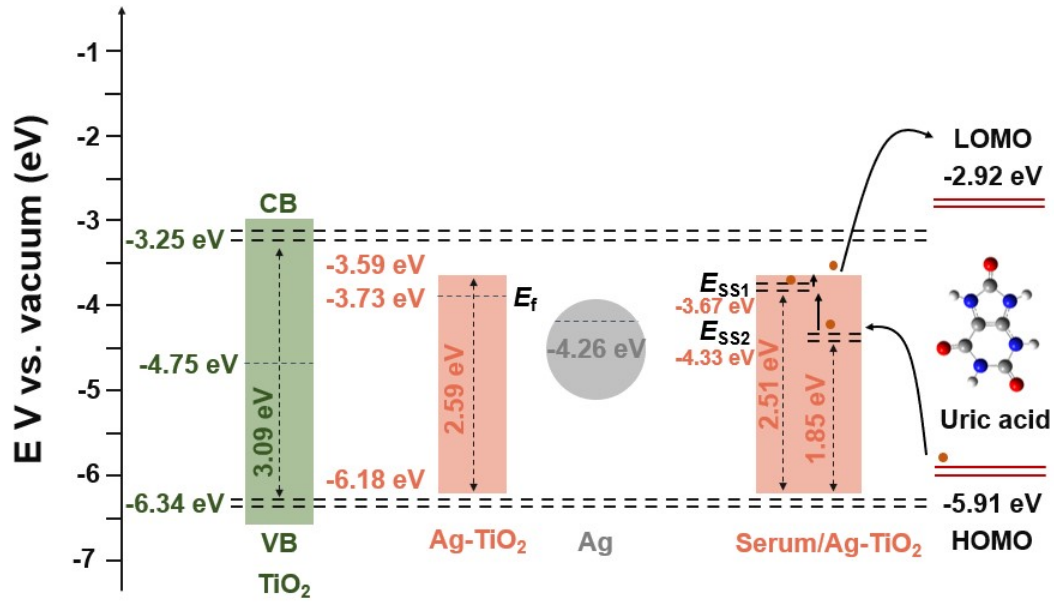

Figure S12. Schematic illustration of charge transfer (CT) between the Ag and Ag-TiO_2 substrates and a uric acid molecule under 785 nm laser excitation.

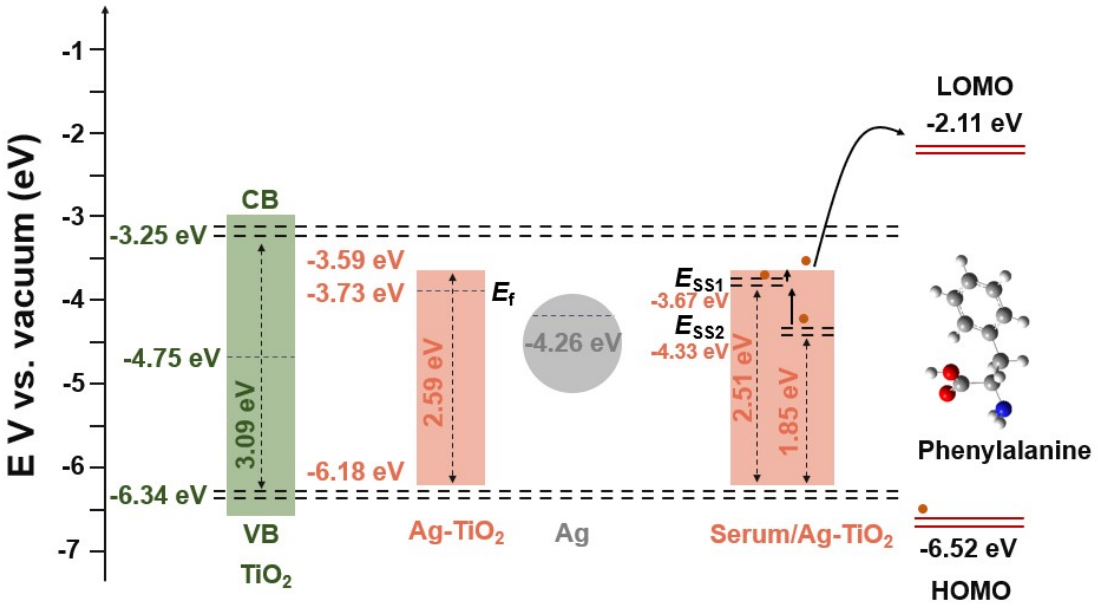

Figure S13. Schematic illustration of charge transfer (CT) between the Ag and Ag-TiO_2 substrates and a phenylalanine molecule under 785 nm laser excitation.

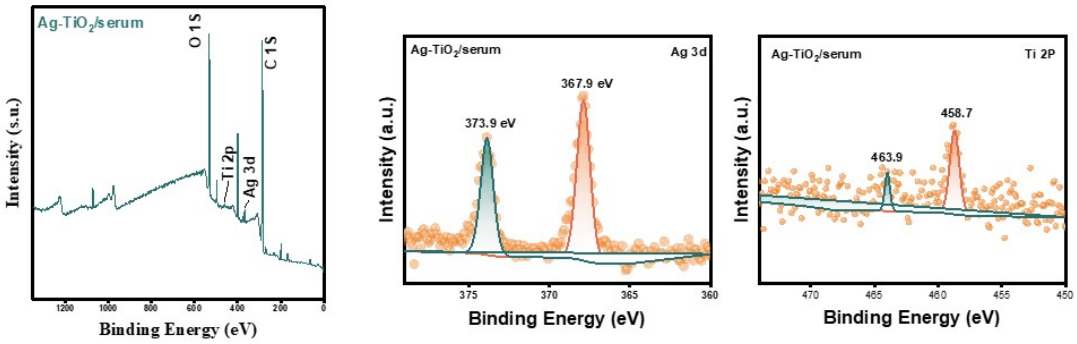

Figure S14. (a) XPS survey spectrum, (b) Ag 3d, and (c) Ti 2p high-resolution spectra of the Ag-TiO_2/WSIF hybrid system.

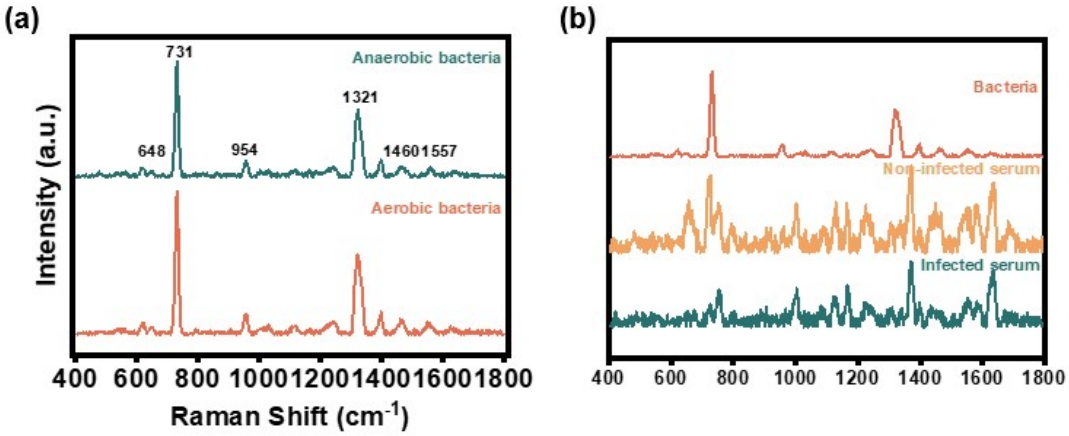

Figure S15. (a) SERS spectra of anaerobic and aerobic bacteria on the Ag-TiO_2 substrate. (b) Comparison of the SERS spectra of infected and non-infected WSIF with those of bacteria, showing that no characteristic bacterial peaks were observed in the WSIF spectra.

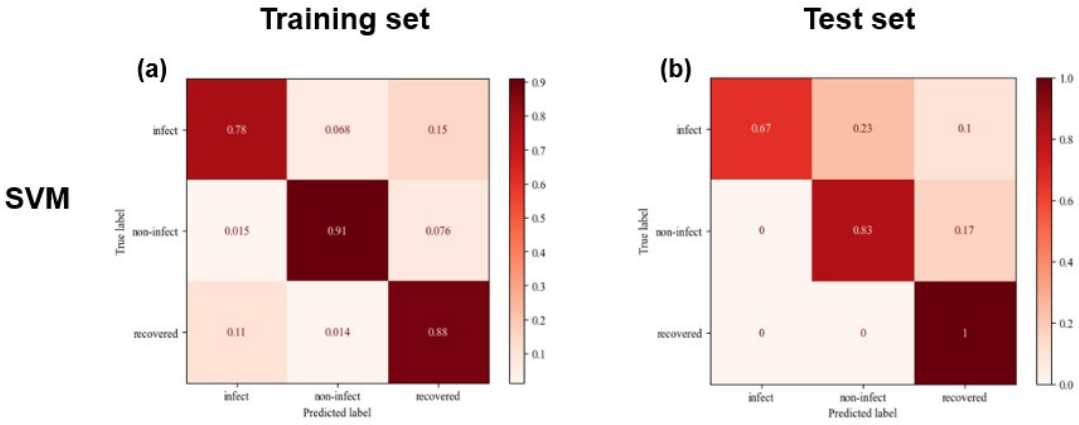

Figure S16. Confusion matrices of the SVM algorithm on the (a) training set and (b) test set.

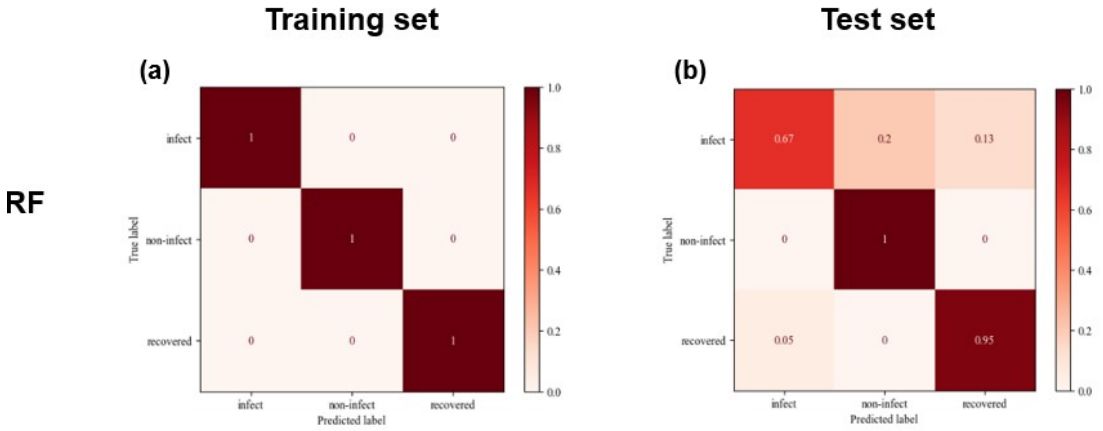

Figure S17. Confusion matrices of the RF algorithm on the (a) training set and (b) test set.

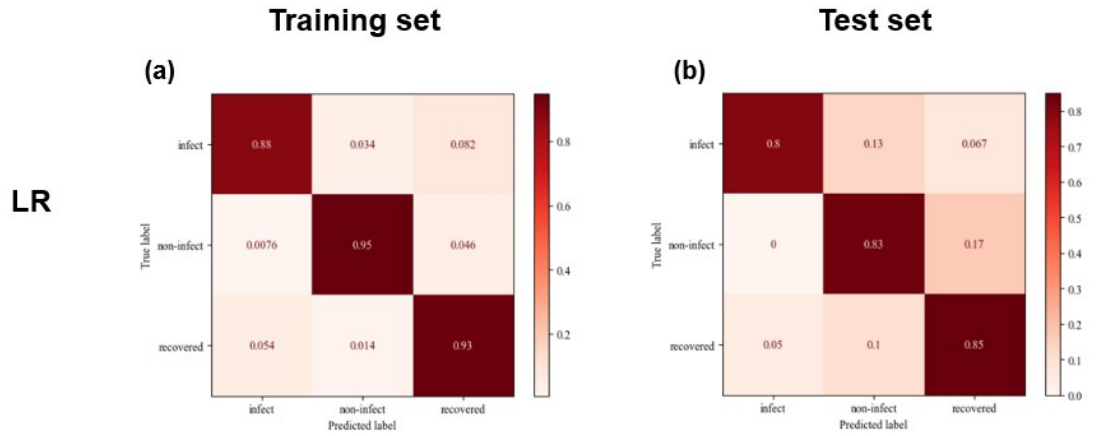

Figure S18. Confusion matrices of the LR algorithm on the (a) training set and (b) test set.

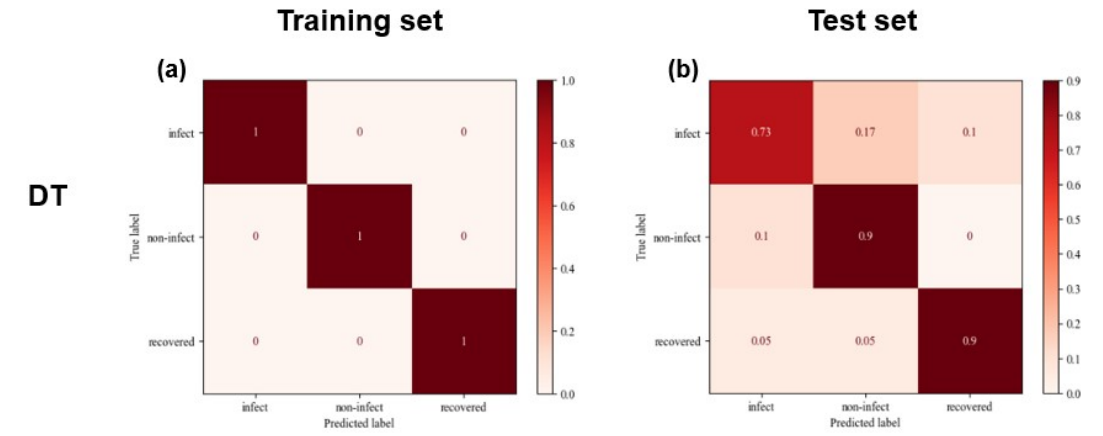

Figure S19. Confusion matrices of the DT algorithm on the (a) training set and (b) test set.

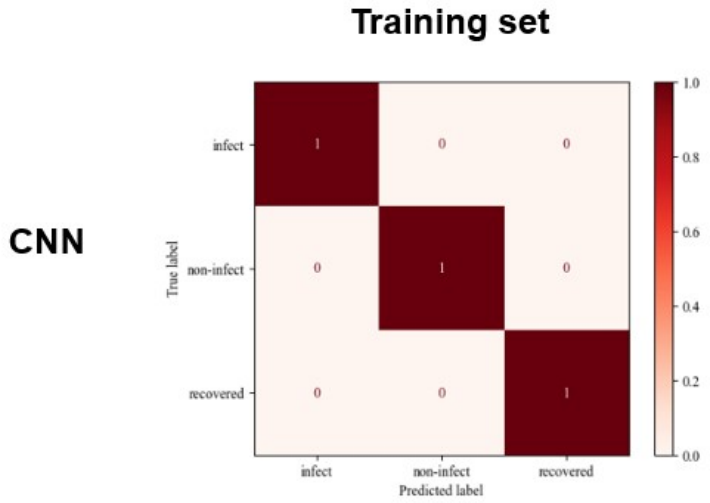

Figure S20. Confusion matrices of the CNN algorithm on the (a) training set.

Table S1. WSIF SERS peak and vibration mode assignments of Ag substrate and Ag-TiO_2 substrate based on the literature[5-8].

Peak position (cm^{-1})	Major assignments	Ag	Ag-TiO_2
624	Phenylalanine	√	√
650	Tyrosine	√	√
723	Hypoxanthine	√	√
742	Thymine	√	√
781	Cytosine	-	√
801	Uric acid	-	√
854	Tyrosine	-	√
893	Uric acid	-	√
954	Amino acids	√	√
1020	Phenylalanine	-	√
1092	Lipid	√	√
1127	Uric acid	-	√
1182	Tyrosine	-	√
1212	Lipid	√	√
1324	Lipid	√	√
1436	Protein	√	√
1579	Phenylalanine	√	√

Note: √: Presence of related substances; -: No related substances.

Table S2. The detailed assignments of tyrosine characteristic peaks[9, 10].

SERS Peak position (cm^{-1})	Major assignments
640	Ring breathing + C-C torsion
846	C-H bending + ring breathing (para-substituted aromatic ring)

1181	C-H in-plane bending
1609	Aromatic C=C symmetric stretching

Table S3. The detailed assignments of uric acid characteristic peaks[11, 12].

SERS Peak position (cm^{-1})	Major assignments
664	N-C-N bending in imidazole ring
907	C-N stretching + ring vibration
1022	Ring breathing / C-C-N modes
1217	C-N-H bending

Table S4. The detailed assignments of phenylalanine characteristic peaks[10].

SERS Peak position (cm^{-1})	Major assignments
1003	Totally symmetric ring breathing
1045	Ring in-plane C-H bending + C-C stretching

Table S5. Performance indicators of the five models on the training set.

Algorithm type	Accuracy	Sensitivity	Precision	F1 score
Logistic regression	0.920	0.920	0.930	0.920
Decision tree	1	1	1	1
Support vector machine	0.854	0.854	0.856	0.854
Random forest	1	1	1	1
Convolutional neural network	1	1	1	1

Table S6. Performance indicators of the five models on the test set.

Algorithm type	Accuracy	Sensitivity	Precision	F1 score
Logistic regression	0.825	0.825	0.840	0.828
Decision tree	0.838	0.838	0.838	0.836
Support vector machine	0.813	0.813	0.847	0.811
Random forest	0.863	0.863	0.876	0.856
Convolutional neural network	0.956	0.956	0.958	0.956

Table S7. Demographic and clinical information of osteomyelitis and control groups.

Variable	Osteomyelitis (n = 20)	Fracture without infection (n =20)
Sex		
Male	15	13
Female	5	7
Comorbidities		
Hypertension	4	2
Diabetes	5	0
Coronary heart disease	3	0
Lifestyle factors		
Smoking	4	3
Drinking	3	3

Reference:

[1] Y. Zhou, Q. Gu, T. Qiu, X. He, J. Chen, R. Qi, R. Huang, T. Zheng, Y. Tian, Ultrasensitive Sensing of Volatile Organic Compounds Using a Cu-Doped SnO2 -NiO p-n Heterostructure That Shows Significant Raman Enhancement*, Angew. Chem. Int. Ed. Engl. 60(50) (2021) 26260-26267. https://doi.org/10.1002/anie.202112367.

[2] T. Sun, Y. Wu, H. Ma, C. Zhang, C. Li, B. Man, C. Yang, Z. Li, The Design of WTe2/Graphene/Ag NPs Heterostructure for the Improvement of the Chemical Enhancement in SERS, Nano Lett. 24(48) (2024) 15324-15330. https://doi.org/10.1021/acs.nanolett.4c04339.

[3] J.R. Lombardi, R.L. Birke, A Unified Approach to Surface-Enhanced Raman Spectroscopy, J. Phys. Chem. C 112(14) (2008) 5605-5617. https://doi.org/10.1021/jp800167v.

[4] X. Zou, Y. Dong, J. Ke, H. Ge, D. Chen, H. Sun, Y. Cui, Cobalt monoxide/tungsten trioxide p-n heterojunction boosting charge separation for efficient visible-light-driven gaseous toluene degradation, Chem. Eng. J. 400 (2020) 125919. https://doi.org/https://doi.org/10.1016/j.cej.2020.125919.

[5] Y. Hong, Y. Li, L. Huang, W. He, S. Wang, C. Wang, G. Zhou, Y. Chen, X. Zhou, Y. Huang, W. Huang, T. Gong, Z. Zhou, Label-free diagnosis for colorectal cancer through coffee ring-assisted surface-enhanced Raman spectroscopy on blood serum, J. Biophotonics 13(4) (2020) e201960176. https://doi.org/https://doi.org/10.1002/jbio.201960176.

[6] C. Carlomagno, M. Cabinio, S. Picciolini, A. Gualerzi, F. Baglio, M. Bedoni, SERS-based biosensor for Alzheimer disease evaluation through the fast analysis of human serum, J. Biophotonics 13(3) (2020) e201960033. https://doi.org/https://doi.org/10.1002/jbio.201960033.

[7] H.F. Nargis, H. Nawaz, H.N. Bhatti, K. Jilani, M. Saleem, Comparison of surface enhanced Raman spectroscopy and Raman spectroscopy for the detection of breast cancer based on serum samples, Spectrochimica Acta Part A: Molecular and Biomolecular Spectroscopy 246 (2021) 119034. https://doi.org/https://doi.org/10.1016/j.saa.2020.119034.

[8] H. Jin, Q. Lu, S. Jin, Z. Song, Y. Zou, H. Ding, H. Gao, X. Chen, Research on Measurement Conditions for Obtaining Significant, Stable, and Repeatable SERS Signal of Human Blood Serum, IEEE Photonics Journal 9(2) (2017) 1-10. https://doi.org/10.1109/JPHOT.2017.2672900.

[9] Y. Lu, D. Lu, R. You, J. Liu, L. Huang, J. Su, S. Feng, Diazotization-Coupling Reaction-Based Determination of Tyrosine in Urine Using Ag Nanocubes by Surface-Enhanced Raman

Spectroscopy, Nanomaterials 8(6) (2018) 400.

[10] F. Madzharova, Z. Heiner, J. Kneipp, Surface Enhanced Hyper-Raman Scattering of the Amino Acids Tryptophan, Histidine, Phenylalanine, and Tyrosine, J. Phys. Chem. C 121(2) (2017) 1235-1242. https://doi.org/10.1021/acs.jpcc.6b10905.

[11] V.R. Kodati, A.T. Tu, J.L. Turumin, Raman Spectroscopic Identification of Uric-Acid-Type Kidney Stone, Appl. Spectrosc. 44(7) (1990) 1134-1136. https://doi.org/10.1366/0003702904086470.

[12] X. Kong, H. Liang, W. An, S. Bai, Y. Miao, J. Qiang, H. Wang, Y. Zhou, Q. Zhang, Rapid identification of early renal damage in asymptomatic hyperuricemia patients based on urine Raman spectroscopy and bioinformatics analysis, Frontiers in Chemistry Volume 11 - 2023 (2023). https://doi.org/10.3389/fchem.2023.1045697.